Electronic structure of a (3×3)-ordered silicon layer on Al(111)

Yusuke Sato [1], Yuki Fukaya [2], Mathis Cameau [3,4], Asish K. Kundu [5], Daisuke Shiga [6,7], Ryu Yukawa [6],
Koji Horiba [6], Chin-Hsuan Chen [8], Angus Huang [8], Horng-Tay Jeng [8,9,10], Taisuke Ozaki [1],
Hiroshi Kumigashira [6,7], Masahito Niibe [1,11] and Iwao Matsuda [1]

[1]*Institute for Solid State Physics (ISSP), The University of Tokyo, Kashiwa, Chiba 277-8581, Japan*
[2]*Advanced Science Research Center, Japan Atomic Energy Agency, 2-4 Shirakata, Tokai, Naka, Ibaraki 319-1195, Japan*
[3]*Institut des NanoSciences de Paris, Sorbonne Université, F-70005 Paris, France*
[4]*Institut de Minéralogie, de Physique des Matériaux et de Cosmochimie, Sorbonne Université, F-70005 Paris, France*
[5]*Istituto di struttura della Materia, Consiglio Nazionale delle Ricerche, Strada Statale 14 km 163.5, Trieste I-34149, Italy*
[6]*Institute of Materials Structure Science, High Energy Accelerator Research Organization (KEK), Tsukuba, Ibaraki 305-0801, Japan*
[7]*Institute of Multidisciplinary Research for Advanced Materials, Tohoku University, Aoba-ku, Sendai 980-8577, Japan*
[8]*Department of Physics, National Tsing Hua University, Hsinchu 30013, Taiwan*
[9]*Physics Division, National Center for Theoretical Sciences, Hsinchu 30013, Taiwan*
[10]*Institute of Physics, Academia Sinica, Taipei 11529, Taiwan*
[11]*Laboratory of Advanced Science and Technology for Industry, University of Hyogo, 3-1-2 Koto,
Kamigori-cho, Ako-gun, Hyogo 678-1205, Japan*

The electronic structure of the (3×3)-ordered phase of a silicon (Si) layer on Al(111) has been studied by angle-resolved photoemission spectroscopy using synchrotron radiation and modeled by a trial atomic model. A closed Fermi surface originating from a linearly dispersing band is identified. A band structure calculation of a trial atomic model of the honeycomb silicene on Al(111) implies that the metallic band originates from the Al-Si hybrid state that has the Dirac-cone-like dispersion curve. The Si layer on Al(111) can be a model system of Xenes to realize the massless electronic system through the overlayer-substrate interaction.

I. INTRODUCTION

Elemental atomic layers have attracted academic interests in their fundamental physics and they have also found significance in technological applications such as next-generation devices [1]. A well-known example is the two-dimensional (2D) honeycomb lattice of carbon, i.e., graphene [2]. In the group-IV element, there have also been reports on silicene (Si), germanene (Ge), and stanene (Sn) [3–10]. These monatomic layers, termed Xenes, have been widely studied because they host Dirac cones at the K (K') points of the Brillouin zone (BZ), which enables exotic quantum devices [3]. However, the existence of such Dirac bands in silicene has been controversial because the layers have been grown on crystal surfaces and the significance of the contribution of the external substrate effect has been debated by researchers [11–16]. Using angle-resolved photoemission spectroscopy (ARPES), Dirac cones of the silicene layer on Ag(111) were observed along zone boundaries in the surface BZ of Ag(111), not at the K (K') points of the silicene BZ [11,14–16]. The electronic structure is described theoretically in terms of the superstructure-induced splitting of Dirac cones by the substrate-overlayer interaction [14]. This result reveals the nature of heterojunctions at the electric contacts between silicene and electrode in, for example, a transistor [17] and also paves the way to manipulate electronic properties of silicene in the external environment.

Silicon deposition has been made on other metal substrates [4,6,11–14,18] and a (3×3)-ordered phase is formed on Al(111) [19–21]. The surface has been known to consist of a silicon overlayer and, thus, it is of interest to investigate the surface electronic structure.

In the present research, we studied electronic states of a silicon layer on Al(111) that forms the (3×3) surface periodicity by ARPES using synchrotron radiation. Electronic bands of the overlayer are identified through a comparison with those of the clean Al(111) surface [22]. Our results show that the overlayer is metallic and the metallic band has linear dispersion curves. The band calculation, based on density functional theory (DFT), is conducted on a trial atomic model of the honeycomb silicene on Al(111). Similarities between the theoretical and experimental band dispersions indicate that the electronic states of the silicon layer likely originate from the Al-Si hybridization, which indicates indispensable substrate-overlayer interaction.

II. EXPERIMENT

A clean Al(111) surface was obtained by cycles of Ar^+ sputtering and annealing, followed by confirmation of crystallinity by observing a low-energy electron diffraction (LEED) pattern and of cleanliness by measuring x-ray photoemission spectroscopy (XPS). Subsequently, Si was deposited on Al(111) at 350 K, which showed the (3×3) LEED

pattern [Fig. 1(a)]. A schematic drawing of the (1×1) surface Brillouin Zone (SBZ) and (3×3) SBZs is depicted in Fig. 1(b). From the XPS measurement of Al 2p and Si 2p core levels, silicon coverage of the surface overlayer is evaluated about 0.4 ML, which is consistent with previous reports on the (3×3)-Si-ordered phase on Al(111) [21].

ARPES measurements of the (3×3)-Si/Al(111) and clean Al(111) surfaces were performed at the VUV-Photoemission beam line (Elettra, Trieste) and at BL-2A (Photon Factory, Japan). The photoemission data were collected using multichannel detection (polar angle) combined with sample rotations (azimuthal or tilt angle) and converted into energy (E)-momentum space (k_x, k_y), where E is the kinetic energy and k_x, k_y are the in-plane components of the wave number (wave vector) that is parallel to the surface.

First-principles calculations were performed using the projector augmented wave (PAW) method [23,24] as implemented in the Vienna Ab initio Simulation Package [25–28] based on density functional theory with the Perdew-Burke-Ernzerhof (PBE) type of generalized gradient approximation (GGA). The 12×12×1 Monkhorst-Pack k mesh and a cutoff energy of 300 eV are used in the self-consistent field calculations. The geometries of all the systems are optimized with the total energies converged within 10^{-4} eV. To study the substrate effect in the Si/Al(111) systems, we adopted a trial honeycomb model by geometrically optimizing a (2×2)-honeycomb silicene lattice on top of a seven-layer Al(111)-(3×3) substrate. As a result of optimization, the honeycomb lattice is slightly distorted. The supercell lattice constant is 8.59 Å and the interlayer distance is 2.25 Å between the silicene layer and the top Al layer. The bond lengths of the two Si-Si bonds in the optimized structure are 2.473 and 2.476 Å.

To compare with the experiment Fermi surface, we unfold the band structures of the silicene-(2×2)/Al(111)-(3×3) supercell Brillouin zone (BZ) to the BZ of the Al(111)-(1×1) unit cell by using the BANDUP package [29]. The Fermi surfaces are derived by tiling the zero-energy contour of the unfolded band structure.

III. RESULTS AND DISCUSSION

Figures 1(c) and 1(d) display the photoemission map at the Fermi level (E_F) of the clean Al(111) and the (3×3)-Si layer on Al(111) with the (1×1) SBZ and symbols of the symmetry points. The intensities of the contours are modulated to give only a threefold symmetry due to the matrix element that is sensitive to the local bonding configuration in the material [30,31]. In Fig. 1(c), Fermi contours of Al bulk bands, b_{Al}, and a surface-resonance/state band, SS_{Al}, of the Al(111) surface are observed, as previously done by ARPES [22]. These states also clearly appear in the (3×3)-Si layer on Al(111) [Fig. 1(d)], indicating that the Al surface resonance/state is likely survived after the Si deposition. It leaves a possibility that the Al(111) surface state, generated in the inverted bulk band gap, is topologically protected as in cases of the noble-metal surface state [32]. In Fig. 1(d), the intensity distributions, except from b_{Al} and SS_{Al}, likely originate from the (3×3)-Si/Al(111) system. Figure 2 shows energy wave-number diagrams along symmetry axes of the Γ-$M'_{1\times1}$ and Γ-$K_{1\times1}$ directions, which are used to trace the

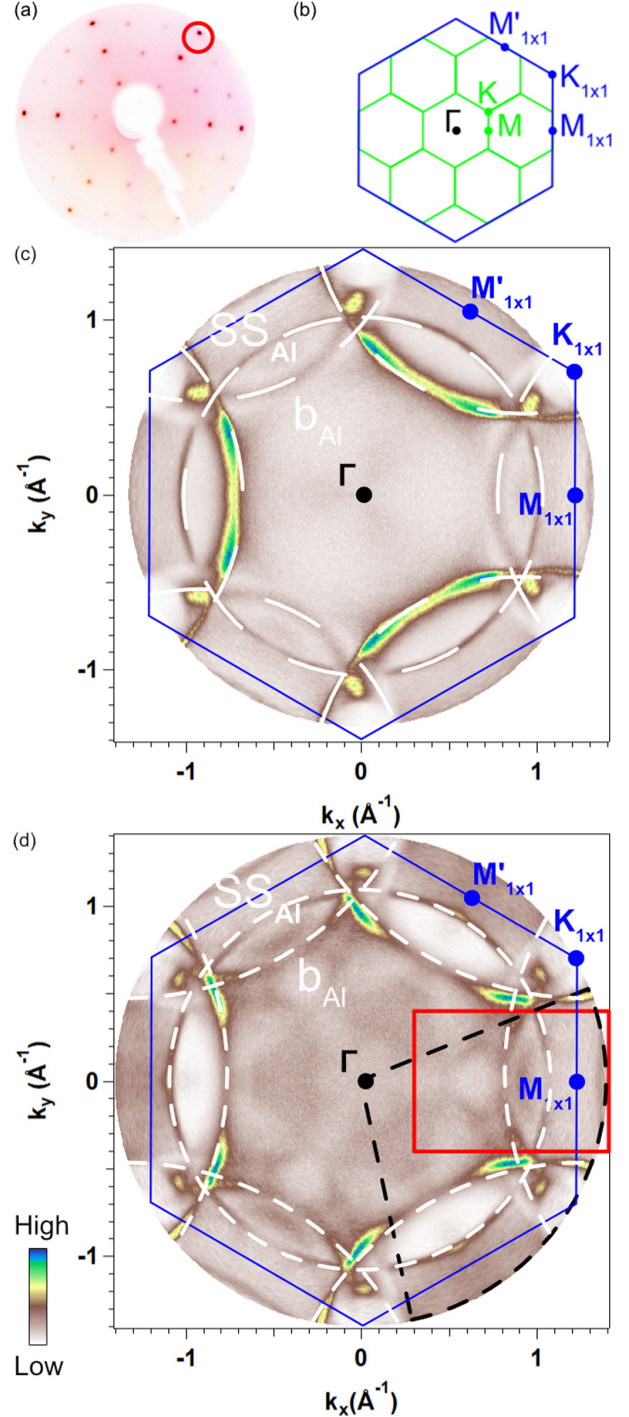FIG. 1. (a) A LEED pattern at electron energy of 88.2 eV of (3×3)-Si/Al(111). The red circle indicates one of the Al(111)-(1×1) LEED spot. (b) A schematic diagram of the surface Brillouin zone (SBZ). The blue and green hexagons correspond to the Al(111)-(1×1) and Al(111)-(3×3) SBZs, respectively. (c) Fermi surface map of clean Al(111) surface taken at $h\nu = 45$ eV and at room temperature. (d) Fermi surface map of (3×3)-Si/Al(111) taken at $h\nu = 47$ eV and at 20 K. The overall mapping is obtained by the symmetric folding of the region surrounded by black dashed curves. Fermi surfaces of the clean Al(111) substrate are traced with white dashed curves. SS_{Al} and b_{Al} correspond to the Fermi surface originating from surface-resonant/state and bulk bands of Al(111). The red square region is focused in Fig. 3(a).
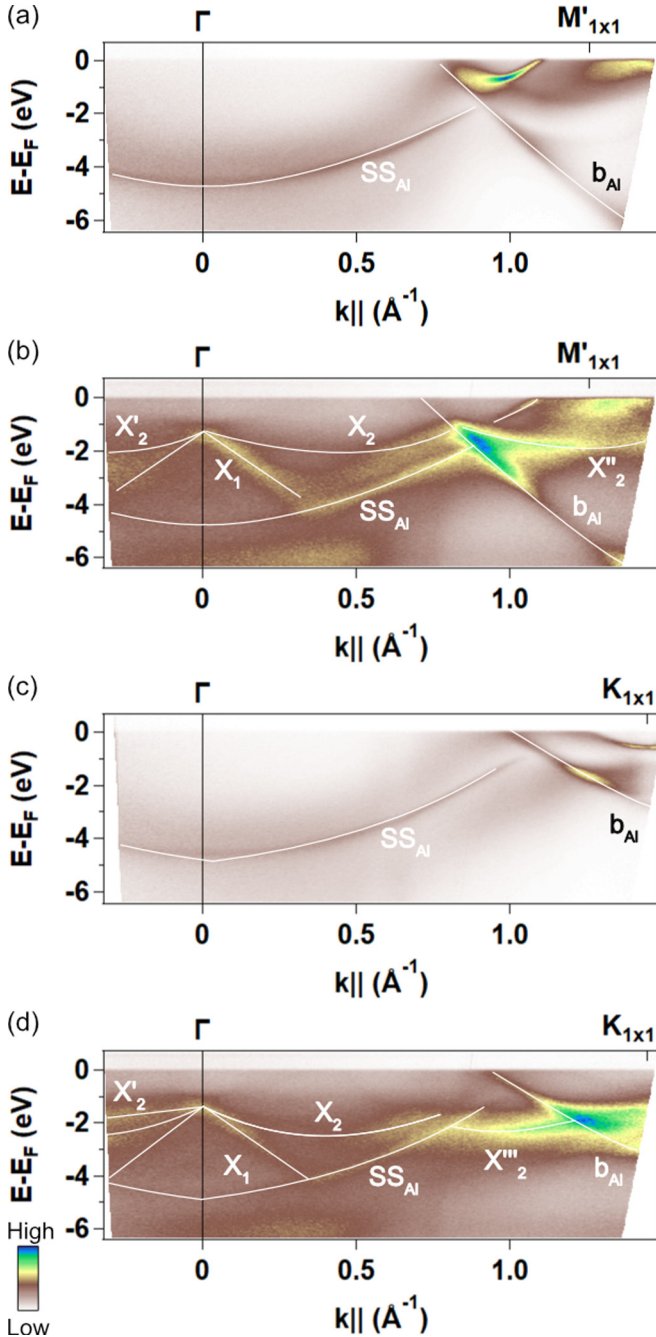
FIG. 2. Band-dispersion plots of (a), (c) clean Al(111) and (b), (d) 3×3-Si/Al(111) along the (a), (b) Γ-M'_{1x1} and (c), (d) Γ-K_{1x1} directions taken at $h\nu = 50$ eV and at room temperature. The white lines are schematic drawings of the observed band-dispersion curves.
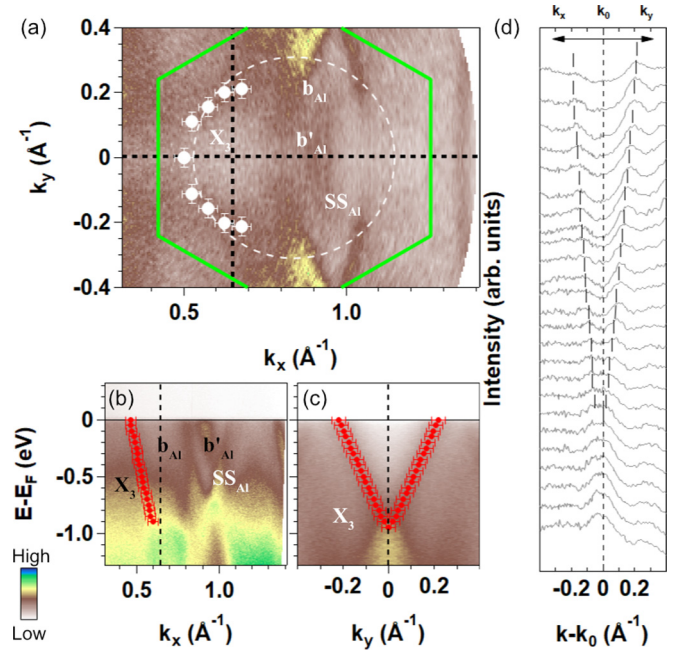

FIG. 3. (a) Fermi surface mapping of (3×3)-Si/Al(111) near the M_{1x1} point taken at 20 K. The green hexagon represents the Al(111)-(3×3) Brillouin zone. The white markers are the positions of the Fermi wave vector of X_3 determined from the peaks in the experimental spectra. The white dashed line represents the estimated Fermi surface contour made by the X_3 band. (b), (c) Band-dispersion plot along (b) $k_y = 0$ Å^{-1} and (c) $k_x = 0.65$ Å^{-1}. The red markers are the positions of the peaks in momentum-distribution curves. (d) Momentum-distribution curves near $k_0 = (0.65, 0)$. The curves shown in $k - k_0 < 0$ are along $k_y = 0$ Å^{-1}, and those in $k - k_0 > 0$ are along $k_x = 0.65$ Å^{-1}. Momentum-distribution curves are taken for each 0.05 eV slice from $E - E_F = 0$ eV to -1.2 eV. All of the error bars correspond to ± 0.03 Å^{-1}.

dispersion curves of the observed features. Two types of bands other than b_{Al} and SS_{Al} can be identified: those that disperse from the Γ point with small (X_1) and with large (X_2, X'_2) effective mass. The X''_2 and X'''_2 bands, observed at large wave numbers, likely share curves with the X_2 (X'_2) band.

Focusing on spectral features of the photoemission Fermi surface around $k_x = 0.65$ Å^{-1}, as shown in the red rectangle in Fig. 1(d), the Fermi surface map is revisited in Fig. 3(a) with the dispersion plots at $k_y = 0$ Å^{-1} [Fig. 3(b)] and $k_x = 0.65$ Å^{-1} [Fig. 3(c)]. The metallic X_3 band with the linear

dispersion and with its crossing point of $E - E_F = -1$ eV can be found at $k_y = 0$ Å^{-1} and $k_x = 0.65$ Å^{-1}. Possible Fermi surfaces of (3×3)-Si/Al(111) are schematically traced in Fig. 3(a), indicating the existence of a closed Fermi surface for the X_3 band.

As shown in Fig. 4, there is another band found at the Γ point. That dispersion has uncertainty due to its shoulder structure positioned at 0.03 Å^{-1} near the Γ point. In momentum-dispersion curves [Fig. 4(b)], the peak positions corresponding to this dispersion are near the position where SS_{Al} could be scattered by the G vector of the Al(111)-(3×3) SBZ. In addition, both the dispersion and SS_{Al} show similar band velocity around 10^6 m/s. From these similarities, the newly observed band is difficult to distinguish from the (3×3)-umklapp replica of SS_{Al}.

To investigate the possible origins of electronic states of (3×3)-Si/Al(111), we conducted a band calculation on a trial atomic model of the honeycomb Si lattice, a silicene layer, on Al(111). The model structure is illustrated in Fig. 5(a). Figure 5(b) shows the dispersion plots with weights of Si atomic orbitals. At binding energies around -2 eV, dispersion curves of light and heavy effective mass can be identified from Γ, as X_1 and $X_2(X'_2)$ in Fig. 2. The agreements between experiments and calculation results imply that the atomic
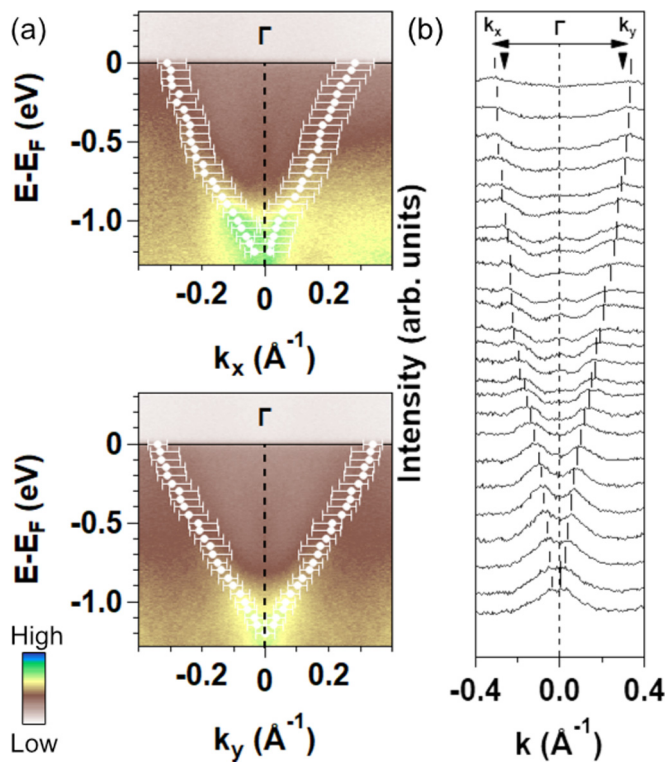
FIG. 4. (a) k_x, k_y band-dispersion plots of (3×3)-Si/Al(111) at the Γ point taken at $h\nu = 47$ eV and at 20 K. The white markers represent the positions of the peaks in experimental spectra. (b) Momentum-distribution curves near the Γ point. The curves shown in $k < 0$ are along $k_y = 0\,\text{Å}^{-1}$, and those in $k > 0$ are along $k_x = 0\,\text{Å}^{-1}$. Momentum-distribution curves are taken for each 0.05 eV slice from $E - E_F = 0$ eV to -1.2 eV. The black triangle markers represent the positions where the umklapp replica of SS_{Al} would appear. All of the wide and narrow error bars correspond to 0.06 and 0.03 Å^{-1}, respectively.

structure may be related to the honeycomb Si lattice and the observed bands originate from $3p_x$ and $3p_y$ orbitals.

Moving onto electronic states near E_F in Fig. 5(b), states mainly with Si $3p_z$ character can be found and they are examined in terms of the external effect [14,33–35]. The band-dispersion curves are complicated because of the Si-Al hybridizations and they have the Dirac-cone-like behavior between the symmetry points (Γ, M). This contradicts the case of a freestanding silicene layer that has Dirac cones at the K points. However, our calculated electronic structure includes the shape of the X_3 band, which indicates that the state likely originates from the overlayer-substrate interaction. Observations of such hybrid states have been reported on borophene/Ag(111) [33] and silicene/Ag(111) [14]. Electronic states with p_z orbitals in the overlayer are greatly influenced by a substrate as compared with those of p_x and p_y. It is naturally understood that the p_z states point to the substrate [14,33,35]. Notably, Feng *et al.* reported that in the tight-binding regime, a pair of Dirac cones in silicene/Ag(111) results from the environmental perturbation to a silicene layer [14].

Furthermore, the calculated electronic structure in Fig. 5(b) shows metallic bands, which is consistent with the ARPES
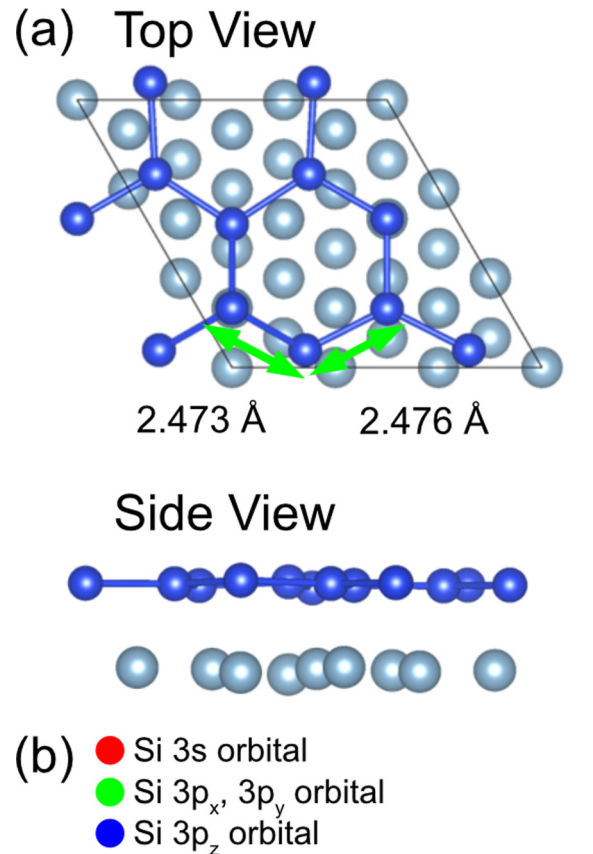

FIG. 5. (a) Schematic drawing of the unit cell of the silicon monolayer with no buckling used in the DFT calculation. (b) Calculated band structure of the silicon layer on an Al(111) substrate. The Al(111) slab has six layers. The characters on the bottom axis correspond to the high-symmetry points of the Al(111)-(3×3) supercell Brillouin zone. The contributions from the Si-$3s$, $3p_{x,y}$, and $3p_z$ orbitals are indicated by the size of the red, green, and blue dots, respectively. A black arrow indicates the band structure compared to the experimental spectra in Fig. 2. A blue arrow indicates the Fermi vector in the calculation that corresponds to that of the X_3 band in Fig. 3.
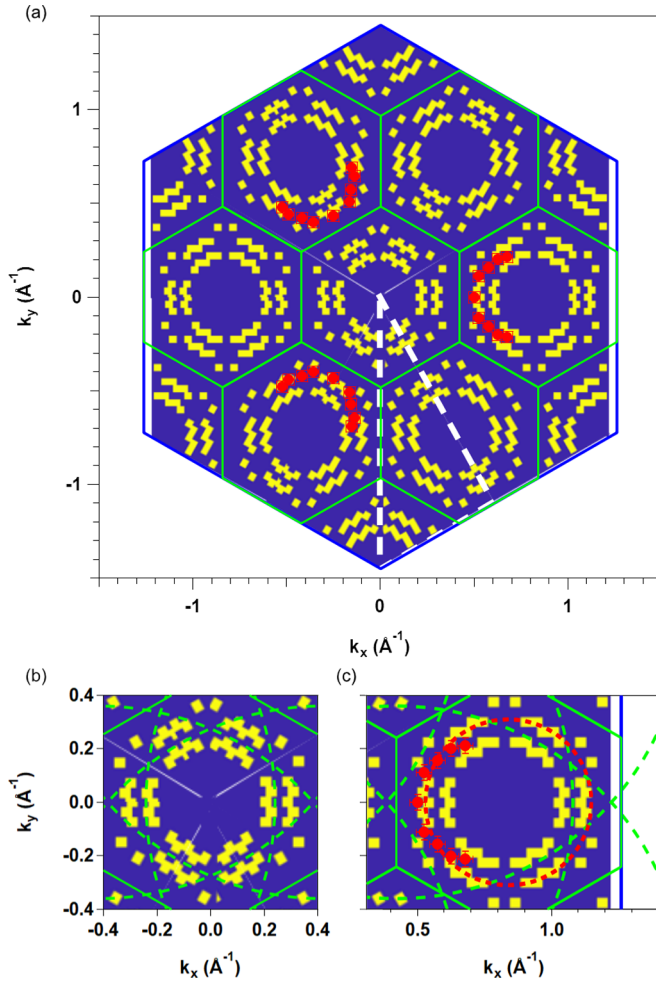
(a)

(b)

(c)

FIG. 6. (a) Fermi surface of the Si/Al(111) constructed by unfolding the band structure of the silicene-(2×2)/Al(111)-(3×3) supercell SBZ to the Al(111)-(1×1) SBZ. Yellow dots show the Fermi wave vector. Red markers represent the experimental Fermi wave vector of X_3. The overall mapping is obtained by the symmetric folding of the region surrounded by white dashed curves. (b) Calculated Fermi surface near the Γ point. The green dashed lines represent the umklapp replicas of the SS_{Al} band in Fig. 1. (c) Calculated Fermi surface near the M_{1x1} point. Red markers represent the experimental Fermi wave vector of X_3. The red dashed line represents the estimated Fermi surface. The green dashed lines represent the umklapp replicas of the SS_{Al} band in Fig. 1. All of the error bars in the experimental points correspond to ± 0.03 Å^{-1}.

observation (Fig. 3). To examine in detail the bands that contain Si orbitals, Fig. 6(a) plots the calculated Fermi surfaces with the Fermi wave-number points depicted by yellow dots, overlaid by the experimental Fermi wave-number points of the X_3 band by red dots. The contours of the theoretical Fermi surface are generated by unfolding the bands calculated in the silicene-2×2/Al(111)-(3×3) supercell SBZ to the Al(111)-

(1×1) SBZ and by tiling the triangular region surrounded by white dashed lines in Fig. 6(a). One can find in the figure a fairly good match between the calculation and the experiment, indicating that the X_3 band may originate from the Si honeycomb layer on Al(111). Figures 6(b) and 6(c) compare the calculated and experimental contours with those of SS_{Al} bands and the replicas in different SBZ. As shown in Fig. 6(c), the Fermi surface of the X_3 band is clearly distinguished, while there are almost complete overlaps between the calculated and the umklapp-scattered bands in the center SBZ [Fig. 6(b)]. This again indicates the difficulty to experimentally extract electronic states of an overlayer on Al(111).

There is fairly good agreement of the metallic band X_3 between experiment and calculation. However, dispersion curves of the other bands are quantitatively different from each other. For example, a degenerate band of X_1 and X_2 at the Γ point is energetically located at -1.5 eV in Fig. 2, while the counterpart in calculation can be found at -2.3 eV in Fig. 5. The Si overlayer on Al(111) has basically the honeycomb structure, but the model may require further modifications such as structural deformation or addition of Si adatoms. A proper understanding of the electronic states requires band calculation, which accounts for the appropriate structure model as obtained by diffraction methods [7,10].

IV. CONCLUSION

We studied the electronic structure of the (3×3)-ordered phase of Si on Al(111) by ARPES using synchrotron radiation and band calculation based on DFT. Electronic states of the Si overlayer are experimentally identified. A closed Fermi surface showing a linear dispersing band or Dirac-cone-like band is observed. By comparing the ARPES spectra with the calculation result of the honeycomb silicene on Al(111), we determined that these electronic bands originate from the Al-Si hybrid states that may be understood in terms of the substrate perturbation of Dirac cones of a silicene, as reported previously [14].

[1] *Monatomic Two-Dimensional Layers: Modern Experimental Approaches for Structure, Properties, and Industrial Use*, edited by I. Matsuda (Elsevier, Amsterdam, 2019).

[2] A. H. Castro Neto, F. Guinea, N. M. R. Peres, K. S. Novoselov, and A. K. Geim, Rev. Mod. Phys. **81**, 109 (2009).

[3] L. Matthes *et al.*, J. Phys.: Condens. Matter **25**, 395305 (2013).

[4] P. Vogt, P. DePadova, C. Quaresima, J. Avila, E. Frantzeskakis, M. C. Asensio, A. Resta, B. Ealet, and G. Le Lay, Phys. Rev. Lett. **108**, 155501 (2012).

[5] A. Fleurence, R. Friedlein, T. Ozaki, H. Kawai, Y. Wang, and Y. Yamada-Takamura, Phys. Rev. Lett. **108**, 245501 (2012).

[6] C.-L. Lin, R. Arafune, K. Kawahara, N. Tsukahara, E. Minamitani, Y. Kim, N. Takagi, and M. Kawai, Appl. Phys. Express **5**, 045802 (2012).

[7] Y. Fukaya, I. Mochizuki, M. Maekawa, K. Wada, T. Hyodo, I. Matsuda, and A. Kawasuso, Phys. Rev. B **88**, 205413 (2013).

[8] M. E. Davila, L. Xian, S. Cahangirov, A. Rubio, and G. LeLay, New J. Phys. **16**, 095002 (2014).

[9] C.-H. Lin, A. Huang, W. W. Pai, W.-C. Chen, T.-Y. Chen, T.-R. Chang, R. Yukawa, C.-M. Cheng, C.-Y. Mou, I. Matsuda, T.-C. Chiang, H.-T. Jeng, and S.-J. Tang, Phys. Rev. Mater. **2**, 024003 (2018).

[10] Y. Fukaya, I. Matsuda, B. Feng I. Mochizuki, T. Hyodo, and S. Shamoto, 2D Mater. **3**, 035019 (2016).

[11] S. K. Mahatha, P. Moras, V. Bellini, P. M. Sheverdyaeva, C. Struzzi, L. Petaccia, and C. Carbone, Phys. Rev. B **89**, 201416(R) (2014).

[12] P. M. Sheverdyaeva, S. K. Mahatha, P. Moras, L. Petaccia, G. Fratesi, G. Onida, and C. Carbone, ACS Nano **11**, 975 (2017).

[13] B. Feng, H. Li, C.-C. Liu, T.-N. Shao, P. Cheng, Y. Yao, S. Meng, L. Chen, and Kehui Wu, ACS Nano **7**, 9049 (2013).

[14] B. Feng, H. Zhou, Y. Feng, H. Liu, S. He, I. Matsuda, L. Chen, E. F. Schwier, K. Shimada, S. Meng, and K. Wu, Phys. Rev. Lett. **122**, 196801 (2019).

[15] C. Lian and S. Meng, Phys. Rev. B **95**, 245409 (2017).

[16] J.-I. Iwata, Y.-I. Matsushita, H. Nishi, Z.-X. Guo, and A. Oshiyama, Phys. Rev. B **96**, 235442 (2017).

[17] L. Tao, E. Cinquanta, D. Chiappe, C. Grazianetti, M. Fanciulli, M. Dubey, A. Molle, and D. Akinwande, Nat. Nanotechnol. **10**, 227 (2015).

[18] B. Feng, B. Fu, S. Kasamatsu, S. Ito, P. Cheng, C.-C. Liu, S. K. Mahatha, P. Sheverdyaeva, P. Moras, M. Arita, O. Sugino, T.-C. Chiang, K. Wu, L. Chen, Y. Yao, and I. Matsuda, Nat. Commun. **8**, 1007 (2017).

[19] F. Jona, J. Appl. Phys. **42**, 2557 (1971).

[20] M. C. Munoz, F. Soria, and J. L. Sacedon, Surf. Sci. **189/190**, 204 (1987).

[21] M. C. Munoz, F. Soria, and J. L. Sacedon, Surf. Sci. **172**, 442 (1986).

[22] S. D. Kevan, N. G. Stoffel, and N. V. Smith, Phys. Rev. B **31**, 1788 (1985).

[23] P. E. Blöchl, Phys. Rev. B **50**, 17953 (1994).

[24] G. Kresse and D. Joubert, Phys. Rev. B **59**, 1758 (1999).

[25] G. Kresse and J. Hafner, Phys. Rev. B **47**, 558 (1993).

[26] G. Kresse and J. Hafner, Phys. Rev. B **49**, 14251 (1994).

[27] G. Kresse and J. Furthmüller, Comput. Mater. Sci. **6**, 15 (1996).

[28] G. Kresse and J. Furthmüller, Phys. Rev. B **54**, 11169 (1996).

[29] P. V. C. Medeiros, S. Stafström, and J. Björk, Phys. Rev. B **89**, 041407(R) (2014).

[30] M. De Santis, M. Muntwiler, J. Osterwalder, G. Rossi, F. Sirotti, A. Stuck, and L. Schlapbach, Surf. Sci. **477**, 179 (2001).

[31] H.-J. Neff, I. Matsuda, M. Hengsberger, F. Baumberger, T. Greber, and J. Osterwalder, Phys. Rev. B **64**, 235415 (2001).

[32] B. Yan, B. Stadtmüller, N. Haag, S. Jakobs, J. Seidel, D. Jungkenn, S. Mathias, M. Cinchetti, M. Aeschlimann, and C. Felser, Nat. Commun. **6**, 10167 (2015).

[33] B. Feng, O. Sugino, R.-Y. Liu, J. Zhang, R. Yukawa, M. Kawamura, T. Iimori, H. Kim, Y. Hasegawa, H. Li, L. Chen, K. Wu, H. Kumigashira, F. Komori, T.-C. Chiang, S. Meng, and I. Matsuda, Phys. Rev. Lett. **118**, 096401 (2017).

[34] C. Liu, I. Matsuda, R. Hobara, and S. Hasegawa, Phys. Rev. Lett. **96**, 036803 (2006).

[35] M. Cameau, R. Yukawa, C.-H. Chen, A. Huang, S. Ito, R. Ishibiki, K. Horiba, Y. Obata, T. Kondo, H. Kumigashira, H.-T. Jeng, M. D'angelo, and I. Matsuda, Phys. Rev. Mater. **3**, 044004 (2019).